DEUTSCHES ELEKTRONEN-SYNCHROTRON

DESY 96–169
August 1996

Higher Order Mode Damping by Artificially Increased Surface Losses

M. Dohlus, H. Hartwig, N. Holtkamp
Deutsches Elektronen-Synchrotron DESY, Hamburg

S. Ivanov, V. Kaljuzhny
Moscow Engineering Physics Institute MEPI, Moscow, Russia

A. Naboka
Institute of Nuclear Research INR, Moscow, Russia

ISSN 0418-9833

NOTKESTRASSE 85 - 22607 HAMBURG

To be sure that your preprints are promptly included in the
HIGH ENERGY PHYSICS INDEX,
send them to (if possible by air mail):

DESY
Bibliothek
Notkestraße 85
22607 Hamburg
Germany

DESY-IfH
Bibliothek
Platanenallee 6
15738 Zeuthen
Germany

DESY 96-169
August 1996

ISSN 0418-9833

Contents

Higher Order Mode Damping by Artificially Increased Surface Losses

M.Dohlus, H.Hartwig, N.Holtkamp[1],
S.Ivanov, V.Kaljuzhny[2],
A.Naboka[3]

[1] Deutsches Elektronen Synchrotron Notkestr. 85, 22607 Hamburg, Germany
[2] Moscow Engineering Physics Institute, MEPI Kashirskoe shosse, 31, 115409 Moscow, Russia
[3] Institute of Nuclear Research, INR Profsojuznaja 7a, 117312 Moscow, Russia

Abstract

It is proposed to use artificially increased losses in the iris holes to damp higher order modes (HOM) in disc-loaded travelling wave structures. To this the irises are covered by a thin metallic layer with low conductivity. The effect of this coating can be described by perturbation theory using the surface impedances of the covered and uncovered areas und the surface current distribution of the modes in a perfectly conducting structure. The losses of travelling wave solutions in periodic structures are calculated by this method for the accelerating mode and for dipole modes. A discrete network model is used to estimate the damping of resonant modes in the first dipole band of the aperiodic SBLC structure. Although the quality factor of the fundamental mode is reduced by a few percent the accelerating field is decreased only by a fraction of this amount when the tapering is modified so that the fill time remains constant. The properties of different coating materials have been investigated by measurements in 1-cell and 6-cell test resonators. For some coating materials the required surface resistivity could be achieved or exceeded, but the effect of heat treatment during brazing has to be taken into account. The first high power tests have been carried out sucessfully. Further measurements will be necessary to get more precise information about the material properties and high power capabilities.

Formula Symbols

fundamental mode characteristics:

P_a	=	input power
P_b	=	power at the end of the travelling wave section
τ_{fill}	=	fill time
$Q^{(m)}$	=	quality factor of the accelerating mode
τ	=	damping parameter ($\tau = 0.5 \ln(P_a/P_b)$)
$Q_0^{(m)}$	=	$Q^{(m)}$ without iris coating
τ_0	=	damping parameter without iris coating
E_{acc}	=	design accelerating field
V_i	=	voltage per cell
$< V_i >$	=	mean voltage per cell
$< V_i >_0$	=	mean voltage per cell without iris coating
k_i	=	synchronous loss-parameter of cell i
$< k_i >$	=	mean synchronous loss-parameter
$< k_i >_0$	=	mean synchronous loss-parameter without iris coating
W_i	=	energy in cell i
L	=	length of one cell (33.34 mm)
P_i	=	power flow through cell i
$v_{gi}^{(m)}$	=	group velocity of cell i
ω	=	2π operation frequency
N	=	number of cells
σ	=	bunch length

dipole mode characteristics:

$Q^{(d)}$	=	quality factor of a dipole mode
$Q_0^{(d)}$	=	$Q^{(d)}$ without iris coating
$k_s^{(d)}$	=	synchronous loss-parameter of cell i

iris coated cells:

d_{coat}	=	see fig. 1
t_{coat}	=	thickness of coating
α	=	geometry on mode dependent absorption parameter
t_{skin}	=	skin depth
μ	=	permeability
κ	=	conductivity
γ	=	propagation constant
P	=	material dependent absorption parameter
P_∞	=	absorption parameter for $t_{\text{coat}} >> _{\text{skin}}$

1 Introduction

Although the interaction between beam and fundamental mode (beam loading) is by far the strongest multi-bunch effect, it can be handled well by choosing an appropriate mode of operation (e.g. staggered timing or shaped klystron pulses). In contrast to this, the higher order mode effects depend strongly on alignment and geometrical tolerances and need special measures to prevent multi-bunch beam break-up or emittance dilution: besides cell-to-cell and structure-to-structure detuning together with active alignment techniques the additional damping of higher order modes is required in most design studies [2],[3],[4],[5]. Effective HOM damping in long travelling wave structures with either one or a few dampers is limited by the existence of trapped modes and the low velocity of the energy propagation. Therefore different concepts of every-cell-dampers with strong impact to the structure design have been proposed [8],[5]. An alternative to this is to increase the surface resistivity of parts of the resonator so that the performance of the accelerating mode is decreased slightly, but the most harmful HOMs are sufficiently damped [1]. In sections 2 and 3 we will show that it is possible to fulfill the requirements of beam dynamics simulations without changing the cell geometry by applying additional losses in the area of the iris hole by surface coating (see fig. 1).

The theoretical analysis of this technique is quite simple, but in practice it has to fulfill certain requirements:

- The iris covering is exactly at the location with the highest field strength. For the very conservative SBLC design field strength of 17MV/m, one can expect approximately 40MV/m at the curvature of the iris hole. For the unloaded gradient of 21MV/m a field strength of 50MV/m can occur and an upgrade with doubled input power would lead to 70MV/m (without beam loading). Although these values have been by far exceeded in S-band copper cavities with very smooth and clean surfaces [6] it is not obvious that they can be reached by materials with the necessary conductivity properties.
- For an effective and selective damping the surface resistance of the coated area has to be increased by a factor 10 to 20. Therefore the ratio μ/κ of the covering material has to be 100 to 400 times higher compared to the basic material (copper) and the thickness of the layer has to be at least in the order of the skin depth. This limits the choice of materials and it seems most likely that this conditions can be fulfilled only with $\mu_r > 1$.
- The process used for the covering has to be able to deposit a layer of the required material on a particular part of a curved surface with a very low roughness and reproducable thickness t_{coat}. Especially if t_{coat} is used to control the surface resistivity it is necessary to obtain a thickness in the order of 5 to 10μm with an accuracy of approximately 1μm. Additionally the coating has to endure a acid bath before brazing and then several brazings at temperatures of 850 degrees and more.

2 Theoretical Investigation

2.1 Concepts of Selectivity

A main design criterion for HOM dampers is the selectivity: the performance of the accelerating mode should be unchanged or only minimally decreased while all other modes that are responsible for instabilities or emittance dilution have to be sufficiently damped. In the case of the SBLC structure the accelerating mode is a travelling wave monopole mode and the cumulative beam break-up is essentially driven by the modes of the first dipole passband ([2],[4]). To distinguish between these fields two concepts of selectivity are available:

- frequency selectivity and
- "field-pattern" -selectivity.

The frequency selectivity is illustrated in fig. 2 with an discrete network model of a double resonator that can oscillate in a symmetric (monopole) and an anti-symmetric (dipole) mode. Fig. 2b represents high-pass filtering as it is usually realized by coupling to a waveguide with the cut-off frequency above the fundamental mode. The asymmetry in this picture is analogue to the asymmetry caused by a single coupling hole at one side of the resonator. The system in fig. 2c is separated from the absorber by a band-stop filter. This corresponds to choke mode cavities as proposed by Shintake [5]. Both techniques are able to cover a wide frequency range if a broad-band load can be realized. In contrast to this, the band-pass coupling in fig. 2d is used to match one (or a few) dipole mode resonance(es) to the surface resistance of the absorbing resonator. All these dampers require additional reactive elements to fulfill the frequency selectivity. Even if the load is perfectly separated from the fundamental mode and the additional reactive elements are loss free, a part of the fundamental mode energy is stored in the filter elements and is therefore not available for acceleration. For example, if the selectivity is given by the cutoff frequency of a waveguide, the field at the operation frequency leaks through the coupling hole and decays exponentially into the waveguide. This leads in some cases to a very high field strength in the coupling slots.

The "field-pattern" selectivity can be achieved with a coupling hole that disturbs the current distribution in the cavity walls minimally. Another possibility is to make use of symmetries: if the fundamental mode of the absorber waveguide is anti-symmetric to the accelerating field but compatible with the dipole field, no frequency separation has to be utilized. Of course, higher waveguide modes may need the frequency selectivity, but this is less critical because their cut-off frequencies are well separated from the operation frequency. An example with discrete elements is shown in fig. 2e.

Usually the absorber is an independent component, but selectivity is achievable even with artificially increased losses at parts of the resonator surface. The magnetic energy distribution of the accelerating mode in a SBLC cell in fig. 3a has the lowest surface currents at the curvature of the iris hole. Although the distribution in fig. 3b represents only one of many possible patterns in the frequency range of the first dipole band, the high losses in the iris hole are typical for almost all of them. Therefore dipole modes are much more sensitive to increased losses in the iris hole than the accelerating field.

For the rest of this report we will consider iris-coated SBLC cells as shown in fig. 1. We will find later that the required damping can be reached by increasing the real part of the surface impedance by a factor of 10 to 20. This is still possible with metallic materials. All damping effects are well described by pertubation theory so that the numerical analysis is extremely simplified.

2.2 Resonator with Partially Covered Surface

The quality factor of a resonant mode ν in a cavity with small surface losses can be calculated by

$$Q_\nu = \omega_\nu \frac{\int_V \mu \left|\vec{H}_\nu\right|^2 dV}{\int_A \mathrm{Re}\left\{\vec{E}_\nu \times \vec{H}_\nu^*\right\} dA}. \tag{1}$$

The electrical field in the surface integral is eliminated using perturbation theory and the surface impedance[1] Z_S which relates the perpendicular $\vec{E}$- and $\vec{H}$-field components. For a resonator which is bounded either by the basic cavity material (surface 1) or by a covered area (surface 2) the quality factor can be expressed as a function of mode and material properties:

$$Q_\nu(P) = \frac{Q_{0\nu}}{1 + \alpha_\nu \cdot (P-1)}. \tag{2}$$

The "geometry and mode dependent absorption parameter"

$$\alpha_\nu = \frac{\int_{A_2} |\vec{H}_\nu|^2 dA}{\int_A |\vec{H}_\nu|^2 dA} \tag{3}$$

is independent of material properties. $Q_{0\nu}$ the quality of the cavity without covering is determined by the surface impedance Z_{S1} (of the basic cavity material), the tangental $\vec{H}_\nu$ distribution and the stored energy. The "surface absorption parameter"

$$P = \frac{\mathrm{Re}\{Z_{S2}\}}{\mathrm{Re}\{Z_{S1}\}} \tag{4}$$

describes the absorption capability of the covered area in comparison to the cavity material.

If the thickness t_{coat} of the covering is large compared to the skin depth t_{skin1} the absorption parameter P is frequency independent[2] given by

$$P_\infty = \sqrt{\frac{\kappa_1 \mu_2}{\kappa_2 \mu_1}}. \tag{5}$$

In the more general case of a homogeneous layer with finite thickness t_{coat} the absorption parameter follows as

$$P = P_\infty \mathrm{Re}\left\{(1+j)\frac{P_\infty \sinh(\gamma_2 t_{\mathrm{coat}}) + \cosh(\gamma_2 t_{\mathrm{coat}})}{P_\infty \cosh(\gamma_2 t_{\mathrm{coat}}) + \sinh(\gamma_2 t_{\mathrm{coat}})}\right\} \tag{6}$$

[1] The surface impedance is defined for a plane wave perpendicular to a plane surface.
[2] In the following equations μ and κ are asumed as frequency independent (and real).

with

$$\gamma_2 = \sqrt{j\omega\kappa_2\mu_2} = \frac{1+j}{t_{2\text{skin}}} \ .$$

This function is plotted in fig. 4 for several values of P_∞. The maximal absorption is obtained for $t_{\text{coat}} \simeq 1.6 \cdot t_{2\text{skin}}(\omega_{\text{HOM}})$. For this and for smaller coating thickness the absorption parameter of the fundamental mode is slightly smaller leading to a slight improvement of the selectivity. In thicker layers the difference between $P^{(m)} = P(\omega_{\text{acc}})$ and $P^{(d)} = P(\omega_{\text{HOM}})$ is almost negligible.

The covered area (surface 2) and the geometry parameter d_{coat} are defined in fig. 1 for SBLC cells. (For all calculations d_{coat} was set to 1.5mm.) Fig. 5 shows the quality of the accelerating mode and one particular dipole resonance for cell 25 (with $v_g/c_0 = 3.7\%$) of the tapered SBLC structure. As expected the covering is mode selective: for P of the order of 10 the monopole mode losses are increased by a few percent but the dipole mode quality is reduced to a small fraction.

2.3 Damping in SBLC Cells

In this section we calculate "single cell properties" of the accelerating monopole mode ($2\pi/3$ phase advance) and of dipole modes in the first passband. These properties are derived from travelling wave (TW) and standing wave (SW) fields which fulfill the boundary conditions in an stack of identical cells. The monopole field in a cell of the tapered structure is very close to the corresponding single cell TW field, but the dipole modes are standing modes and their field pattern is aperiodic. Nevertheless dipole quality factors of single cells can be used to estimate the quality of trapped modes in the SBLC structure.

a) Q and α as a function of the cell number

The TW quality factors of the accelerating $2\pi/3$ monopole and $\pi/3$ dipole mode are shown in fig. 6 for every cell of the SBLC structure. The $\pi/3$ dipole mode was chosen because it is approximately in the middle of the passband and typical for most modes in this band. The absorption of the accelerating mode is almost constant ($Q^{(m)} \simeq 14000$) for all cells of a section. The quality factor of the dipole modes rises with the cell number and frequency from 13000 to 16000 but the mean value is almost the same as for the monopole mode.

Due to the different magnetic energy distribution in fig. 3 the α coefficients of monopole modes are much smaller than for dipole modes (fig. 7). The numbers for cell 25 (with $v_g^{(m)}/c_0 = 3.7\%$) have just been used to calculate fig. 5. If the iris losses in this cell are ten times increased the power dissipation of the accelerating mode rises only 4.5% but the dipole mode $Q^{(d)}$ is reduced from 13514 to 3027.

b) Q and α as function of the frequency (phase advance)

The frequencies and quality factors of dipole modes in a six cell resonator terminated by perfect conducting planes in the middle of the first and last iris are shown in figs. 8 and 9. The $Q^{(d)}$ value of cell 25 (with $v_g^{(m)}/c_0 = 3.7\%$) without coating is almost constant (13260 to 13530) but for an iris with the absorption property $P = 10$ the quality decreases with the frequency from

4039 for the $5\pi/6$-mode to 2448 at the $\pi/6$-mode. This is different in cells with smaller group velocity such as cell 124 (with $v_g^{(m)}/c_0 = 2.2\%$): even without covering, the quality rises from 14050 ($5\pi/6$-mode) to 18540 (0-mode), but for $P = 10$ these values are reduced only to 4590 and 13850. If the absorption in the iris is increased so that we obtain the same fundamental mode Q reduction as for cell 25, we obtain comparable $Q^{(d)}$ values for most of the frequency band, however the selectivity is drastically reduced for modes close to the upper cut-off frequency. We will see in section 2.4 that this does not significantly lower the damping capabilities for the modes with high loss-parameter.

c) Estimation of HOM damping in a tapered structure

To get a rough approximation for the global HOM damping it is reasonable to assume that modes in the tapered structure are damped similarly to the single cell $\pi/3$ solutions. In the formulas for the monopole and dipole Q reduction

$$\begin{aligned} \frac{Q^{(m)}}{Q_0^{(m)}} &= \frac{1}{1+\alpha^{(m)}(P^{(m)}-1)} \\ \frac{Q^{(d)}}{Q_0^{(d)}} &= \frac{1}{1+\alpha^{(d)}(P^{(d)}-1)} \end{aligned} \tag{7}$$

the surface absorption parameter is only weakly frequency dependent ($P^{(m)} \simeq P^{(d)}$) so that it can be eliminated and we find a direct relation between the Q-reductions:

$$\frac{Q^{(m)}}{Q_0^{(m)}} = \frac{1}{1+\frac{\alpha^{(m)}}{\alpha^{(d)}}\left(\frac{Q_0^{(d)}}{Q^{(d)}}-1\right)}. \tag{8}$$

The selectivity is determined by the ratio of the α coefficients that is drawn in fig. 11. The α-ratio increases slightly towards the end of the structure but it can almost be taken as constant. This means that, if the surface absorption parameter P is adjusted in every iris so that the fundamental mode is damped by a constant amount, all dipole modes will be reduced by the same factor. This damping performance is plotted in fig. 11.

For example: if one wants to keep the losses of the accelerating mode at 5% one has to increase the absorption parameter from $P = 10$ to $P = 21$ from the begining to the end of the section. With a "typical α-ratio" of 0.016 one can expect to reduce a dipole mode quality from approximately 15000 by a factor of 1/4.3 to 3500.

2.4 Damping of HOMs in the SBLC structure

A fast and effective method to estimate the field distributions and losses in the tapered SBLC structure uses discrete coupled oscillator models. As the lowest two dipole bands interact strongly with each other, the effects in this frequency range cannot be sufficiently modelled and explained by one resonator (representing one mode) per cell. We follow the approch of [9] and relate the lowest TM- and TE-like fields to LC oscillators. To keep the model simple we neglect the coupling between resonators of the same cell and regard only

magnetic coupling to neigbouring cells. This is justified by the mode symmetry and the fact that most of the field energy in the regions of the coupling holes is stored in the magnetic field. Fig. 12 shows the equivalent network. The resonators in the upper chain correspond to TM-like fields, the resonators in the lower chain to TE-like modes. The longitudinal and transversal electric fields are represented by capacitors in the longitudinal and transversal directions. As losses in the resonators and the coupling elements are taken into account, the eigenvalue equation takes the following form:

$$\begin{aligned} &\left(p\underline{\mathbf{M}}_{(n,n-1)} + \underline{\mathbf{R}}_{(n,n-1)}\right) \quad \underline{\mathbf{i}}_{(n-1)} \\ &+ \left(p\underline{\mathbf{L}}_{(n)} + \underline{\mathbf{R}}_{(n)} + 1/p\underline{\mathbf{C}}_{(n)}^{-1}\right) \quad \underline{\mathbf{i}}_{(n)} \\ &+ \left(p\underline{\mathbf{M}}_{(n,n+1)} + \underline{\mathbf{R}}_{(n,n+1)}\right) \quad \underline{\mathbf{i}}_{(n+1)} \quad = 0 \end{aligned} \tag{9}$$

with

$$\begin{aligned} \underline{\mathbf{i}}_{(n)} &= \begin{pmatrix} I_{1,(n)} \\ I_{2,(n)} \end{pmatrix}, \\ p &= -2\omega/Q + j\omega. \end{aligned}$$

If one normalizes all capacitors to 1 and keeps the symmetry suggested in fig. 12 this model has ten degrees of freedom: five degrees concerning the dispersion characteristics of the loss free cells and five degrees to simulate power disipation. The free parameters are determined so that the dispersion and damping properties at the 0-,$\pi/2$- and π-mode frequencies in the first dipole band and the 0- and π-mode frequencies of the second band are set to the values from MAFIA simulations. Thus we we get a very good simulation of properties in the first passband and a reasonable accuracy in the second.

Fig. 13 shows the loss-parameters of the first 180 dipole modes. Among these only the lowest 143 modes contribute substantially to the long range wake. Therefore we call these 143 modes between 4.134GHz and 4.447GHz "strong coupling modes". The Q values for three different surface absorption parameters P are plotted in fig. 14 and some statistical data of the strong coupling modes are compared in table 1. In the last section we estimated some general dipole mode properties from the $\pi/3$ mode characteristics of individual cells. Indeed the ($Q^{(d)}_{\pi/3}$,cell number)-distribution in fig. 6 is very similar to the ($Q^{(d)}$,frequency)-distribution of modes in the undamped detuned structure. The highest $Q^{(d)}$-value of the strongly coupling modes is 16100, the mean value is close to the quality of the accelerating field. On the other hand, the data points in fig. 14 for $P = 1$ and $P = 10$ can be compared with the results for 6-cell resonators: at the begining of the band the losses decrease very similarly to those in fig. 8, for high frequencies we get values like those in fig. 9. The qualitatively different behaviour of some modes between 4.46GHz and 4.54GHz is caused by a coupling to fields in the second passband. This effect is less important because no strong coupling mode is affected. The mean quality factor of strong coupling modes is decreased to 3860 for $P = 10$ and to 2141 for $P = 20$.

By variing the material properties or the thickness t_{coat} of the coating layer (or even d_{coat}) it is possible to get the same additional losses in every cell for the

accelerating mode. To increase the losses in this way by 5% (10%) one needs P values between 10 (21) and 21 (45). Fig. 15 shows the $Q^{(d)}$ distributions for this type of covering. The $Q^{(d)}$ values in the frequency range from 4.22GHz to 4.44GHz are almost constant. The mean quality factor of strong coupling modes of 3109 (1669) is slightly better than that estimated above.

2.5 Reduced Accelerating Field

For a constant gradient structure the fill time τ_{fill}, the damping parameter τ and the quality factor $Q^{(m)}$ of the accelerating mode are related by

$$\tau_{\text{fill}} = \frac{2\tau Q^{(m)}}{\omega} \ . \tag{10}$$

If the fill time is kept constant the reduced quality factor of the accelerating mode needs an increased damping parameter and a change of the group velocity profile along the structure. As the damping parameter τ is increased more of the input power is available for the absorption inside the structure ($P_a - P_b = P_a(1 - \mathrm{e}^{-2\tau})$) and therefore the additional losses caused by the coating are partially compensated. The voltage per cell can be directly calculated from the structure parameters:

$$\begin{aligned} V_i &= 2\sqrt{k_i W_i} \\ &= 2\sqrt{k_i L P_i / v_{gi}^{(m)}} \\ &= 2\sqrt{k_i (P_a - P_b) Q^{(m)}/(\omega N)}. \end{aligned} \tag{11}$$

The effect of the relative Q reduction $x = Q^{(m)}/Q_0^{(m)}$ is given by:

$$V_i = \sqrt{k_i}\sqrt{x(1 - \mathrm{e}^{-2\tau_0/x})}\ 2\sqrt{Q_0^{(m)} P_a/(\omega N)}. \tag{12}$$

Only the loss-parameter k_i depends on the cell index. As it increases with decreasing iris holes the voltage per cell is not quite constant (which is in contradiction to the term "constant gradient"). Fig. 16 shows the loss-parameter as function of the group velocity. The complete structure is described by the mean voltage per cell:

$$< V_i > = < \sqrt{k_i} > \sqrt{x(1 - \mathrm{e}^{-2\tau_0/x})}\ 2\sqrt{Q_0 P_a/(\omega N)}. \tag{13}$$

For a fast estimation we neglect the x dependency of $< \sqrt{k_i} >$ so that we can directly relate the reduced accelerating voltage to the relative Q reduction:

$$\frac{< V_i >}{< V_i >_0} = \sqrt{x \frac{1 - \mathrm{e}^{-2\tau_0/x}}{1 - \mathrm{e}^{-2\tau_0}}}. \tag{14}$$

This function is plotted in fig. 17. If the fundamental mode $Q^{(m)}$ is reduced by 5% (10%) the mean gradient is only decreased by 1.16% (2.42%). The structure has to be tapered from $v_g^{(m)}/c_0$ =4.16% to 1.33% (4.27% to 1.28%) and therefore $< \sqrt{k_i} >$ is slightly decreased. The exact values of reduced gradients are listed in table 2. Even with beam loading the performance is decreased by only 1.3% (2.6%) compared to an undamped structure with the same fill time.

2.6 High Frequency Effects

a) Damping of higher dipole bands

The second dipole band can also be analysed by the coupled oscillator model. Only a few modes with loss factors as high as those for modes of the first band were found. As their loss-parameter is still a fraction of the peak value in fig. 13 no additional damping seems to be necessary. Nevertheless it can be seen in fig. 18 for cell 25 that the quality parameter of the second dipole band (from 4.5GHz to 5.5GHz) is reduced to a third or less for most of the frequency range.

There are several difficulties for the analysis of higher dipole modes: the cell asymmetry cannot be neglected, coupler cells have to be modeled more precisely, passband regimes may overlap[3] and waveguide modes in the beam pipe come above cut off frequency[4]. The first three problems can be solved by using more advanced field calculation methods or by more complex coupled oscillator models. The last problem is more severe because the problem domain can no longer be treated as closed and the modal theory for which loss-parameters are defined is not valid (or needs modifications).

A practicable way to come to an estimation are single cell calculations leading to synchronous loss-parameters $k_s^{(d)}$ and to $Q^{(d)}$ factors as used in section 2.4. Therefore dipole passbands of several SBLC cells have been computed in the frequency range up to 16GHz. The $Q_0^{(d)}$ distributions in fig. 18 are very different from band to band but their mean values increase approximately linearly with frequency so that the decay time $2Q_0^{(d)}/\omega$ is of the same order $\simeq$ 0.6 to 1μs for all modes[5]. For this reason and due to the Panofsky Wenzel theorem [10] individual passbands contribute to the transverse wakefield proportionally to $k_s^{(d)}/\omega$. The maximal synchronous loss-parameter in the investigated frequency range is found for the lowest band. Only band three and six have values of the same order [11]. Although the Q reduction by iris coating is less effective for higher bands the decay times are reduced to $\simeq$ 0.4...0.8μs. The values at the synchronous frequency for band one, three and six are 0.29μs, 0.29μs and 0.38μs. In the first microsecond the strongest contributions to the wake are given by these bands. Later the effects of higher bands with smaller loss-parameters but higher decay times become dominant if no further absorption mechanism such as power dissipation through the beam pipe is taken into account.

b) Short range monopole wake (resistive wall wake)

To compare the additional wake caused by the iris coating with the short range wake of a loss free cavity we consider a simplified three cell model such as the one calculated in [12].

For high frequencies the impedance of the perfectly conducting cavities decays asymptotically with $\omega^{-1/2}$. Therefore the short range wake of a gausian

[3] E.g. passband 11 and 12 in fig. 18 overlap, passband 13 overlaps with itself.

[4] Lowest cut off frequency of the SBLC beam pipe is 5.7GHz.

[5] This is a very rough estimate for this frequency range. For very high frequencies the quality is probably limited by $g(\text{geometry}) \cdot \omega^{0.5}$.

bunch with the length σ scales[6] as

$$W(t) = \frac{f(t/\sigma)}{\sqrt{\sigma}} .$$

The absolute peak value is $3 \cdot 10^{13} \cdot \sqrt{100\mu\text{m}/\sigma}$ V/C.

The wake caused by the iris coating behaves very similarly to the resistive wall wake in an infinite beam pipe. This has been verified by time domain calculations with a spatial resolution in the conductive material better than the skin depth at $3\omega_\sigma = 3c_0/\sigma$. To reduce the numerical effort the scaling law

$$Z(j\omega) \sim \sqrt{\omega\mu/\kappa} \sim P_\infty\sqrt{\omega}$$

was verified and used. In this context we refer to the surface impedance approximation, assume $\kappa \gg j\omega\epsilon$ and neglect the frequency dependency of the conductivity. As only a short iris and not the infinite beam pipe is concerned it is not appropriate to use the exact solution (reported in [14],[15]). Furthermore the difference between the surface impedance approximation and the exact solution is negligible for the SBLC design bunch length of 0.3mm. Due to the asymptotic $\omega^{+1/2}$ behaviour the contribution of the iris coating to the wake is given by

$$W_{P_\infty}(t) = \frac{g(t/\sigma)}{\sigma^{3/2}}$$

with $g(t) \propto \dot{f}(t)$. The numerical calculation for the model in [12] with two covered irises leads to peak values of $2 \cdot 10^{10} \cdot (100\mu\text{m}/\sigma)^{3/2} \cdot P_\infty$ V/C.

For the SBLC design bunch length the contribution of the iris covering to the short range wake is negligible. For bunches as short as 1μm the resistive wall wake of the covering reaches the same order as the wake of a perfectly conducting cavity, but in this case the resistive wall wake of the uncovered area has to be taken into account as well as the frequency dependency of the material properties.

3 Measurements

3.1 Measurement Setups

Two test resonators have been used for low power Q measurements. The one cell setup in fig. 19 was originally designed for quality control and to check the cell radius. As a dipole resonance ($f \simeq$4.3GHz) can also be measured, this device is used to test single cell quality factors. A quantitative measurement of absorption properties is not possible because the contact resistance of the contact spring (fig. 19 part 2) and the surface resistance of the bottom plate and the body with the cutoff pipe (fig. 19 part 3 and 5) are unknown. Nevertheless the measurements are reproducible so that qualitative comparisons are possible.

The six cell resonator in fig. 20 allows the simulation of field patterns very similar to the fields in the real structure. A measurement reflects the properties

[6] In [12] a scaling with $\sigma^{-0.47}$ was found, but for simplicity we take the exponent 0.5 that is expected from the diffraction model [13].

of all five covered cells so that it is almost inpossible to extract the effect of an individual cell. The highest measurement uncertainties are given by the contacts between the cells (defined by the mechanical pressure) and the effect of the termination by brass-planes in the center of the first and last iris. Fig. 21 shows the influence of the contact pressure on the quality factor of monopole and dipole modes. Especially the $2\pi/3$ and $5\pi/6$ monopole modes are very sensitive: even for a pressure from 600N/mm^2 to 900N/mm^2 the Q-factor increases by $\delta Q \simeq 1000$ with almost constant slope. All measurements have been done with a pressure of 600N/mm^2 to prevent damage to the contact edges. As the Q reduction at monopole frequencies is expected to be in the order of 5% ($\delta Q \simeq 700$) only a qualitative and comparative interpretation of the measurements is possible. The effect of the end cells could be eliminated using measurements with n-cell and $2n$-cell resonators, but due to the other errors it is not really possible to improve the accuracy. The situation for dipole measurements is better: the sensitivity to the contact pressure is significantly smaller and the expected Q reduction (from $\simeq 15000$ to $\simeq 3000$) is large in comparison to the uncertainties mentioned above.

3.2 Single Cell Measurements

Initial tests with cells which were completely galvanically covered with titanium, zirconium or alloys such as stainless steel, Kantal [16], TiN, TiCH, ZrN have been carried out. Promising Q reductions together with good mechanical properties even after heat treatment as in the brazing process have been found only for steel and Kantal. The steel cells suffered a significant reduction of the surface impedance during heating, but even the final absorption property ($P \simeq 10$) was high enough to justify further investigations. Kantal, with an estimated surface absorption parameter of $P \simeq 30$, has a good thermal stability and is still used in LINAC structures (e.g. LINAC II at DESY) to increase the fundamental mode losses in the last cells so that the accelerating travelling wave is terminated. The currently used Kantal loads are **not** covered at the iris.

For further experiments cells of two group velocities (cell number 25 and 124 with v_g/c_0=3,7% and 2,2%) have been coated with Kantal and stainless steel. In each case seven cells were sputtered with a nominal thickness $t_{\text{coat}} = 10\mu$m and a width $d_{\text{coat}} = 1.5$mm. During this process the rest of a cell was protected by a shield.

Fig. 22 and fig. 23 show the Q factors of monopole and dipole modes measured in the one cell test resonator before and after heat treatment. Some statistical properties are listed in table 3. These results are a first hint that the dipole modes be can be damped much more strongly than monopole modes. The dipole quality factors indicate that the Kantal surface resistivity is increased approximately 15% to 20% after the brazing process. The Q values of steel covered cells were initially very small but they increased after heat treatment approximately threefold. Nevertheless $Q^{(d)} \simeq 3000$ in cells with small group velocity can be sufficient to fulfill the requirements. The quality factors of Kantal cells (with $v_g = const$) are reproducible with an accuracy of 8.2% and better. This is a very encouraging result for the first trial. The reproducibility for steel cells, of about 20%, is much worse and it should be noted that the $Q^{(d)}$

change of individual cells due to heat treatment has a much wider spreads.

3.3 Measurements with the 6-Cell Test Resonator

The measured Q values of the 6-cell test resonator for cavities covered with Kantal and stainless steel are shown in fig. 24 and fig. 25.

The quality factor of the accelerating $2\pi/3$ mode is reduced by 10.5% and 7.6% for Kantal covered cells while the steel covering leads for both cell types to a reduction of only 1.2% . It has been mentioned in subsection 3.1 that the reproducability and measurement accuracy is of the order of 5% so that these values can only be a rough estimate. A better measurement of the fundamental absorption properties under real operation conditions needs a test resonator that is prepared, processed and brazed as in the real structure.

The dipole mode measurements in fig. 25 can be qualitativly compared with the MAFIA calculations in fig. 8 and fig. 9 for $P = 10$. With the exception of the lowest point ($5\pi/6$ mode) the measured distributions are very similar to the theoretical ones. The high 0-mode quality factor of cell 124 in not caused by a reduced surface absorption ratio P but by a low mode and geometry dependent absorption coefficient α.

3.4 Surface Absorption Parameter

Due to imperfections, the six cell measurement setup formula (2) has to be generalised:

$$Q = \frac{Q_0}{P_1(1-\alpha) + P\alpha + R} .$$

Q_0 is the quality factor of a resonator with the same surface properties as in the real LINAC structure. From measurements of the structures of the DESY-LINAC II injector it is known that the theoretical quality factor $Q_0^{(m)}$ of the accelerating mode for $\kappa = 5.8 \cdot 10^7$S/m is reached with an accuracy of 3%. Therefore it seems to be reasonable to use results of the MAFIA calculations for $Q_0^{(d)}$ and α of dipole modes. P is the ratio of the surface resistivity of the covered area to the resistivity of the real accelerating structure. As the test cells may have passed different processes and have been kept for a long time usual laboratory conditions (air) the surface resistivity of the copper body changed and is therefore described by the absorption ratio P_1 (with the same reference material as P). R takes into account additional losses caused by the contacts between the cells, the brass boundaries in the first and last iris and the external losses by the pickup antennas. The unknown absorption parameters are estimated as

$$\begin{aligned} P_1 &= 1.2 \pm 0.1 \\ R &= 0.1 \pm 0.1 . \end{aligned}$$

With these numbers and the measured quality factor $Q^{(d)}$, we can calculate the surface absorption parameter of the covered area:

$$P = \frac{1}{\alpha}\left(\frac{Q_0^{(d)}}{Q^{(d)}} - 1.2(1-\alpha) - 0.1\right) \pm 0.1\left(1 + \frac{2}{\alpha}\right) .$$

Table 4 shows the P values for two different cell types with Kantal and stainless steel covering. With the exception of the numbers for $5\pi/6$ modes the values in every row are equal within the uncertainty of the estimated parameters and the Q measurement accuracy.

For cells with an iris radius of 14.9mm and 12.7mm significantly different absorption parameters P are measured for Kantal (22 and 32) and for steel (17 and 13). As the single cell measurements are in good agreement for a given cell type and material, sputtering different iris geometries probably did lead to different coating thickness t_{coat} and therefore to the observed variation in P. Adjusting the sputtering process parameters could then yield the desired values for P over a sufficient range.

4 Further Steps

The calculations and measurements at low power level have demonstrated that selective damping with coated irises is possible. For further investigations two new test resonators, as shown in fig. 26, have been designed and built.

The test resonator in fig. 26a is designed to allow precise measurement of the surface absorption parameter P. It oscillates at 4.4GHz in the TM_{02} mode which has no wall currents in the upper and lower boundary plane at $r =$ 41.6mm. As a small gap at this position does not influence the quality factor it is possible to insert and exchange probe discs without contact problems. The characteristic properties α and Q of the TM_{02} mode are given analytically. Using a reference measurement with a probe which is prepared and processed in the same way as the SBLC cells, the systematic error due to the unknown surface conditions of the resonator body can be eliminated.

The resonator in fig. 26b is suitable for high power tests. Two SBLC cells are coupled to a standard S-band waveguide by inductive slots. The upper cell, which is the probe cell, can be replaced. The vaccum insulation is provided by indium gaskets. As the two cell resonator is operated in a $\pi/2$ standing wave mode, the resonance frequency is slightly below the operational frequency of the LINAC. MAFIA calculations for the two cell SW field and the three cell TW field are used to relate the maximal iris field strength to the total stored energy per cell:

$$w_2 := \frac{W_{\mathrm{tot}}(2\ \mathrm{cells}, \pi/2\ \mathrm{mode}, \mathrm{SW})}{2} \frac{1}{E^2_{\mathrm{max,iris}}},$$

$$w_3 := \frac{W_{\mathrm{tot}}(3\ \mathrm{cells}, 2\pi/3\ \mathrm{mode}, \mathrm{TW})}{3} \frac{1}{E^2_{\mathrm{max,iris}}}.$$

(These numbers differ by less than 20% .) Therefore the input power

$$P_{\mathrm{test}} = \frac{\omega}{Q_{\mathrm{test}}} \cdot 2 \cdot \frac{(E_{\mathrm{acc}} L)^2}{4 k_i} \frac{w_2}{w_3}$$

is needed to simulate the same iris field strength as for the accelerating field E_{acc}. The synchronous loss-parameter k_i is given in fig. 16 and the quality Q_{test} of the test resonator is measured. First tests with an input power of 900kW to cells of type 25 covered with Kantal and steel have been performed sucessfully. This corresponds to an unloaded accelerating field of 25MV/m.

5 Summary

Theoretical investigations show that it is possible to decrease the mean $Q^{(d)}$ value of dipole modes of the first passband from about 15000 to 3100 while the gradient is decreased by less then 1.3% (the effective shunt impedance is lowered by less than 2.6%). To achieve these values the absorption property of the covering has to be varied with the cell number and the group velocity profile has to be changed. Even with the same absorption property for all cells and the same reduction of the accelerating field the mean quality factor can be damped below 3800. Measurements for two cell types have proven the principle and demonstrated that the required surface properties can be reached with stainless steel and Kantal. First high power tests for to gradient of 25MV/m have been carried out successfully. Further investigations concerning the precise electrical properties, the robustness, the reproducability and high gradient conditions are in preparation.

References

[1] Herminghaus, Euteneuer: CERN.

[2] M.Drevlak: 'New Results on the Beam Dynamics in the SBLC'. Internal Report, M96-01, January 1996.

[3] H. Edwards: 'Status of TESLA Test Facility', LC95, pp. 121-143, April 1995.

[4] K.A.Thompson et al.: 'Design and Simulation of Accelerating Structures for Future Lunear Colliders'. Particle Accelerators, Vol.47,pp. 65-109, 1994.

[5] T.Shintake, K.Kubo, H,Matsumoto, O.Takeda: 'HOM-Free Linear Accelerating Structure for e+e- Linear Collider at C-Band', PAC95, May 1995.

[6] M.Yoshika et.al.:'High Gradient Studies of UHF Room Temperature Cavities at S-Band for Linear Colliders', Proccedings of the 1994 International Linac Conference 1994, pp. 302-304, Aug. 1994.

[7] U.van Rienen: 'Higher Order Mode Analysis of Tapered Disc-Loaded Waveguides using the Mode Matching Technique', Particle Accelerators, 1993, Vol. 41, pp. 173-201.

[8] N.Kroll, K.Thompson, K.Bane, R.Gluckstern, K.Ko, R.Miller, R.Ruth: 'Manifold Damping of the NLC Detuned Accelerating Structure',SLAC-PUB-6660, Sept. 1994.

[9] K.Bane, R.Gluckstern: 'The Transverse Wakefield of a Detuned X-Band Accelerator Structure'. SLAC-PUB-5783. March 1992.

[10] W.Panofsky, A.Wenzel: 'Some Considerations Concerning the Transverse Deflection of Charged Particles in Radio Frequency Fields', Rev. Sci. Instrum. 27, p. 967,1956.

[11] N.Holtkamp: 'Status of S-Band Technology at DESY', LC95, p.133, April 1995.

[12] M. Dehler: 'Numerische Lösung der Maxwellschen Gleichungen auf kreiszylindrischen Gittern', PHD thesis, Technische Hochschule Darmstadt, 1992.

[13] K.Bane, M.Sands:'Wakefields of Very short Bunches in an Accelerating Cavity', SLAC-PUB-4441, Nov. 1987.

[14] K.Bane: 'The Short Range Resistive Wall Wakefields', SLAC-AP-87, June 1991.

[15] A. Piwinsky: 'Wake Fields and Ohmic Losses in Round Vacuum Chambers', DESY HERA 92-11, May 1992.

[16] Trademark

[17] T.Khabiboulline, W.Puntus, A.Naboka, S.Ivanov, N.Holtkamp, G.Kreps: 'S-band Single Cell Diagnostic', Internal Report DESY M-96-03,February 1995.

	Q(mode 1)	Q(mode 143)	min(Q)	mean(Q)	max(Q)
$P = 1$	13460	15098	13460	13988	15098
$P = 10$	3982	4973	3307	3860	4973
$P = 20$	2234	2850	1797	2141	2850
$\frac{Q^{(m)}}{Q_0^{(m)}} := 0.95$	3880	3266	2969	3109	3880
$\frac{Q^{(m)}}{Q_0^{(m)}} := 0.90$	2167	1746	1584	1669	2167

Table 1: Q value statistic for the first 143 modes (with $k' > 10^{15}\mathrm{V}/(\mathrm{Cm}^2)$) for iris coating with constant absorption factor P and with constant reduction of the fundamental mode Q.

Q/Q_0	τ	$v_{g1}^{(m)}/c_0$	$v_{g180}^{(m)}/c_0$	U(0mA)/V	U(100mA)/V	U(300mA)/V
1.00	0.543	4.06%	1.37%	1.285E8	1.210E8	1.060E8
0.95	0.572	4.16%	1.33%	*0.9875	*0.9875	*0.9873
0.90	0.604	4.27%	1.28%	*0.9740	*0.9739	*0.9736
0.80	0.679	4.53%	1.17%	*0.9429	*0.9427	*0.9422
0.70	0.775	4.88%	1.04%	*0.9053	*0.9052	*0.9047

Table 2: Parameters and gradients for structures with iris coating and $\tau_{\mathrm{fill}} = 0.808\mu s$, Q_0=14000.

	monopole before h.	monopole after h.	dipole before h.	dipole after h.
copper 3.7%	8919 ± 60		8662 ± 21	
copper 2.2%	8746 ± 90		8748 ± 75	
Kanthal 3.7%	8395 ± 60	8540 ± 60	1660 ± 170	2030 ± 160
Kanthal 2.2%	8396 ± 74	8356 ± 42	1783 ± 155	2041 ± 66
HG steel 3.7%	7871 ± 132	8904 ± 132	911 ± 186	3052 ± 730
HG steel 2.2%	8254 ± 101	8829 ± 84	1558 ± 280	4603 ± 850

Table 3: Mean value and standard deviation of Q measurements for cell 25 ($v_g/c_0 = 3.7\%$) and cell 124 ($v_g/c_0 = 2.2\%$) with different coating materials (Kanthal and stainless steel) before and after heat treatment (i.e. brazing). Seven cells of each type and material have been measured. The individual Q values are plotted in fig. 22 and fig. 23.

Mode	MAFIA f/GHz	Kanthal P	HG steel P	$\pm 0.1(1+2/\alpha)$
$5\pi/6$	4.167	(42.5)	(23.1)	± 0.9
$4\pi/6$	4.174	22.4	17.0	± 0.8
$3\pi/6$	4.190	21.4	17.5	± 0.7
$2\pi/6$	4.218	21.2	16.6	± 0.6
$1\pi/6$	4.264	21.2	15.3	± 0.5

(a)

Mode	MAFIA f/GHz	Kanthal P	HG steel P	$\pm 0.1(1+2/\alpha)$
$5\pi/6$	4.333	(43.6)	12.5	± 1.0
$4\pi/6$	4.350	33.4	12.7	± 1.0
$3\pi/6$	4.382	32.4	14.3	± 1.0
$2\pi/6$	4.431	32.4	13.1	± 1.0
$1\pi/6$	4.496	30.8	11.1	± 1.3
0	4.542	36.1	9.8	± 5.4

(b)

Table 4: Surface absorption coefficent P measured in the dipole band (after thermal processing). a) cell 25 with $v_g/c_0 = 0.037\%$ b) cell 124 with $v_g/c_0 = 0.022\%$

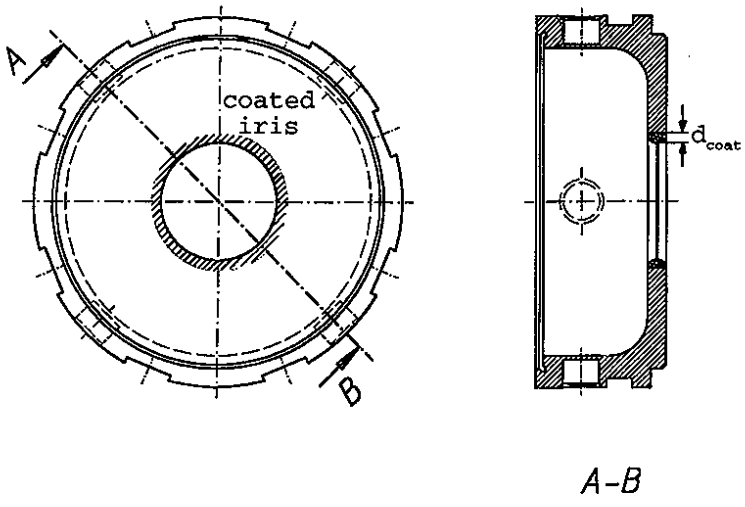

Figure 1: Geometry of the SBLC cell with iris coating.

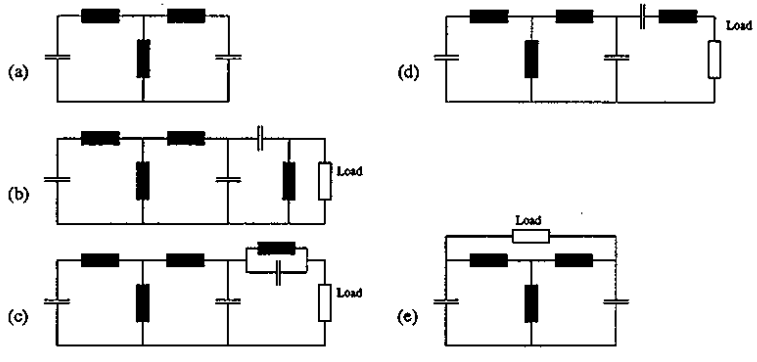

Figure 2: Concepts of selectivity: a) discrete model of a two-mode resonator, b) high pass filtering, c) band stop filtering, d) band pass filtering, e) field pattern selctivity.

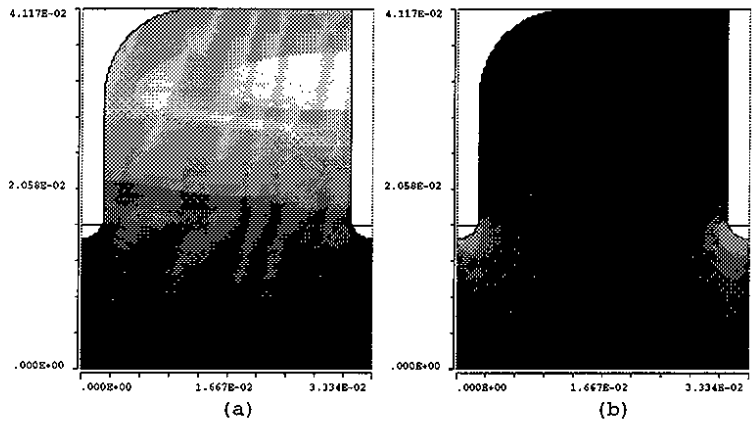

Figure 3: Magnetic energy distribution in one cell of the SBLC structure: a) accelerating mode; b) dipole mode (1st passband, $\pi/3$ travelling wave mode). The surface losses are proportional to the magnetic energy distribution at the surface. The mean energy density is plotted with respect to the time and the azimuthal position. Low energy coresponds to dark gray.

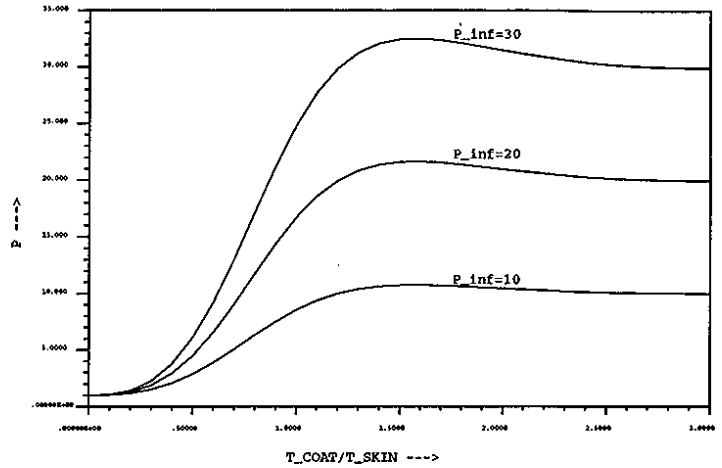

Figure 4: Surface absorption parameter P as a function of the coating thickness t_{coat}.

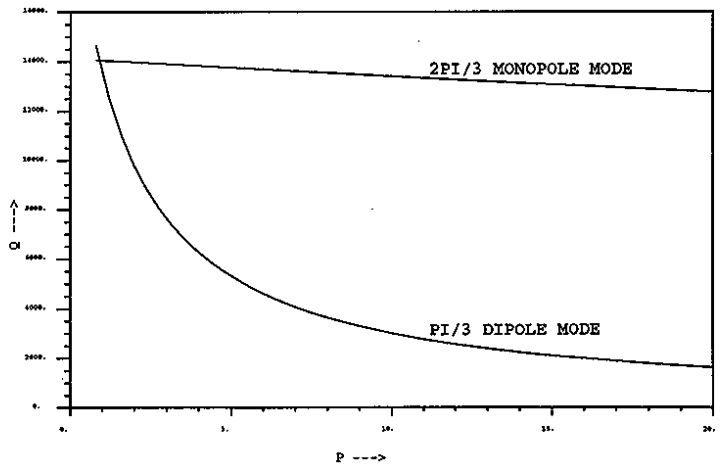

Figure 5: Single cell quality factor of the $2\pi/3$ monopole mode and the $\pi/3$ dipole mode in cell 25 ($v_g^{(m)}/c_0 = 3.7\%$) for different surface conductivity of the coated area (d_{coat} =1.5mm). (The single cell quality factor is calculated for an infinite periodic structure of identical cells.)

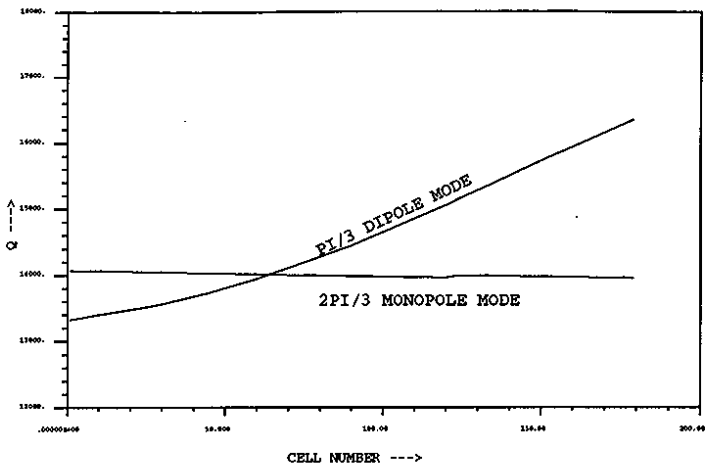

Figure 6: Single cell quality factor of the $2\pi/3$ monopole mode and the $\pi/3$ dipole mode for every cell of the SBLC structure. (The single cell quality factor is calculated for an infinite periodic structure of identical cells.)

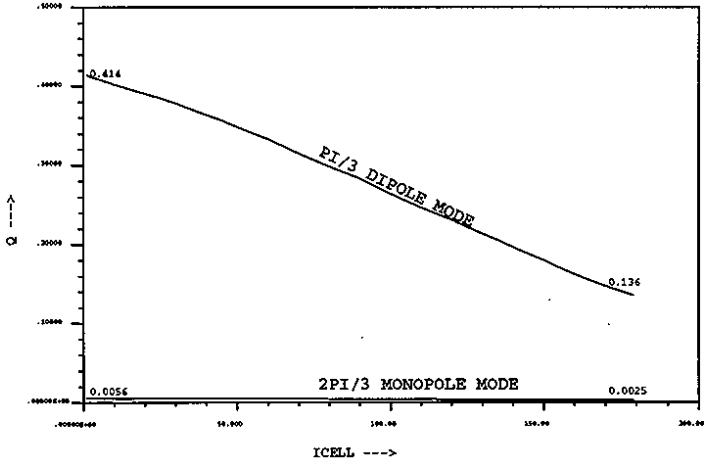

Figure 7: Single cell α factor of the $2\pi/3$ monopole mode and the $\pi/3$ dipole mode for every cell of the SBLC structure (d_{coat} =1.5mm). (The single cell α factor is calculated for an infinite periodic structure of identical cells.)

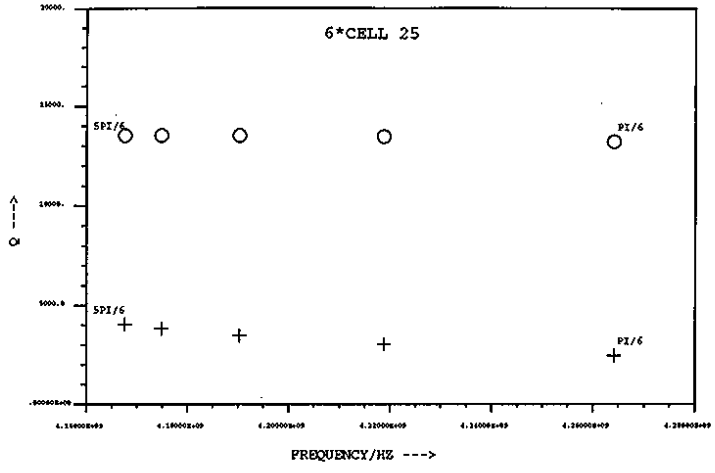

Figure 8: Quality factor of dipole modes in a resonator of six cells with the same dimension as cell 25 in the SBLC structure with (o) and without (+) iris coating ($v_g^{(m)}/c_0 = 3.7\%$, d_{coat} =1.5mm, $P = 10$).

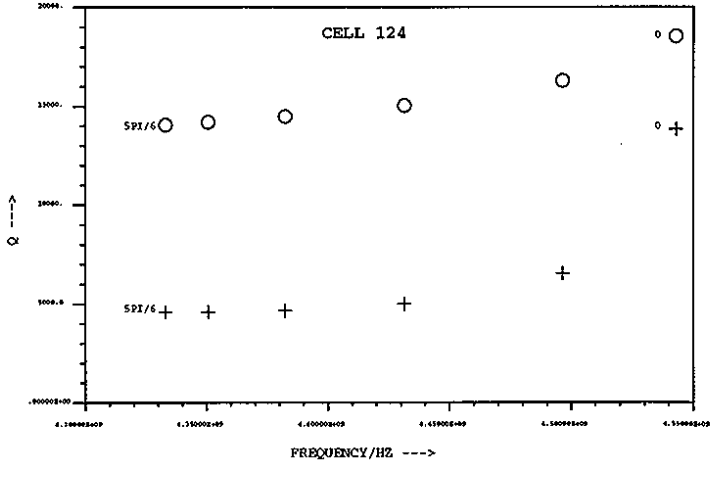

Figure 9: Quality factor of dipole modes in a resonator of six cells with the same dimension as cell 124 in the SBLC structure with (o) and without (+) iris coating ($v_g^{(m)}/c_0 = 2.2\%$, d_{coat} =1.5mm, $P = 10$).

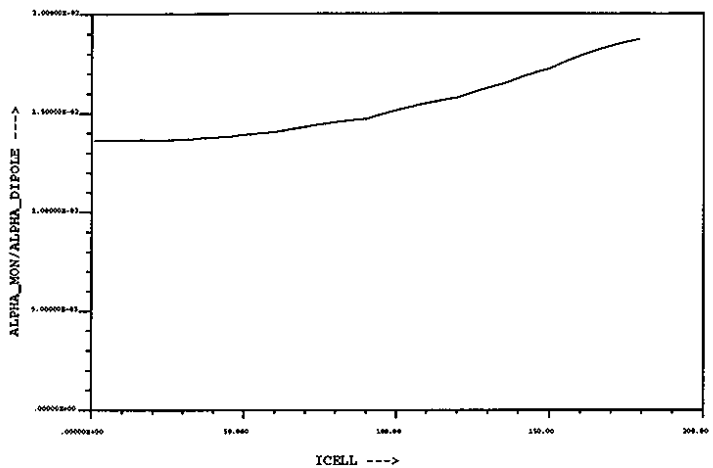

Figure 10: Ratio of the single cell α factors of the $2\pi/3$ monopole and the $\pi/3$ dipole modes for every cell of the SBLC structure (d_{coat} =1.5mm). (The single cell α factors are calculated for an infinite periodic structure of identical cells.)

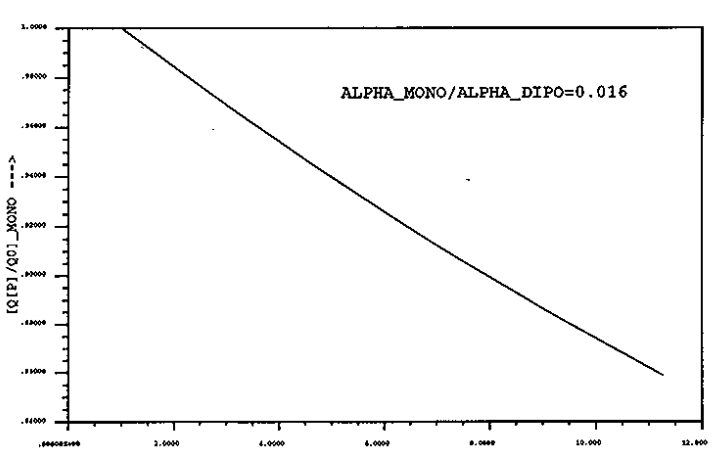

Figure 11: Reduction of the quality factor of the accelerating mode $Q^{(m)}_{\text{coating}}/Q^{(m)}_0$ as a function of the dipole mode supression $Q^{(d)}_0/Q^{(d)}_{\text{coating}}$ for a typical ratio $\alpha^{(m)}/\alpha^{(d)} = 0.016$.

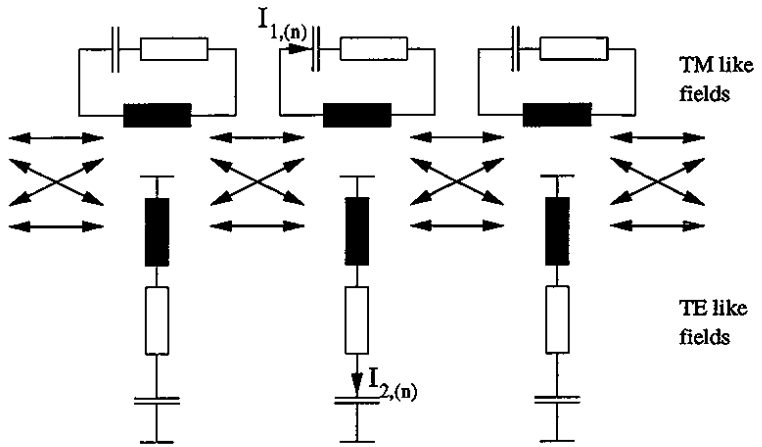

Figure 12: Double-band coupled oscillator model for the dipole modes in a constant gradient structure. The coupling elements include resistive elements that are not drawn in the figure.

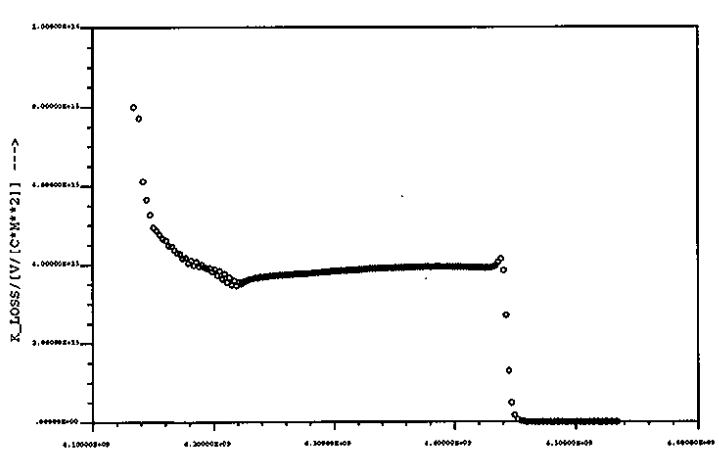

Figure 13: Normalized longitudinal loss-parameters of the first 180 dipole modes in the tapered SBLC structure calculated by an coupled oscillator model.

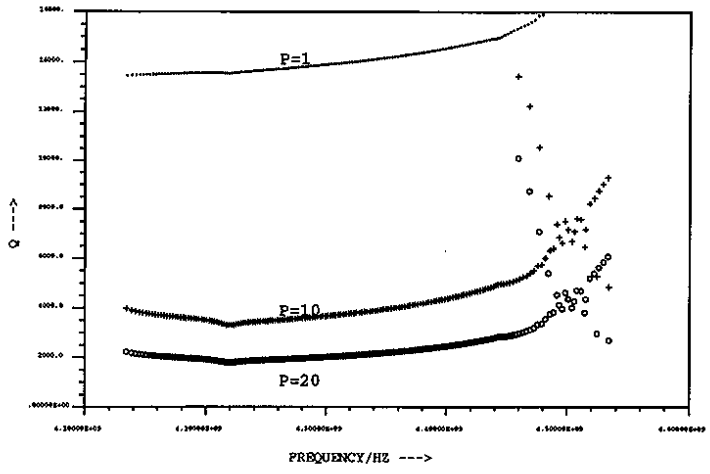

Figure 14: Quality factors of the first 180 dipole modes in the tapered SBLC structure with different iris coating ($P = 1$,$P = 10$,$P = 20$,d_{coat}=1.5mm).

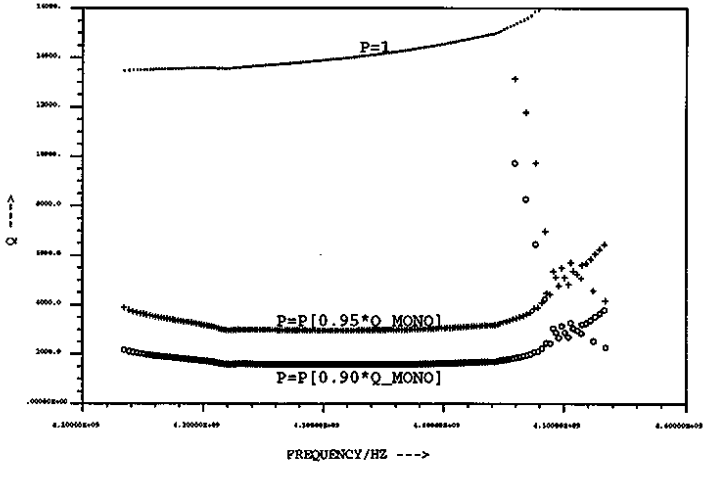

Figure 15: Quality factors of the first 180 dipole modes in the tapered SBLC structure without iris coating and with length dependent coating. P is set for every cell so that the absorption of the accelerating mode is increased in every cell by 5% and 10% (d_{coat}=1.5mm).

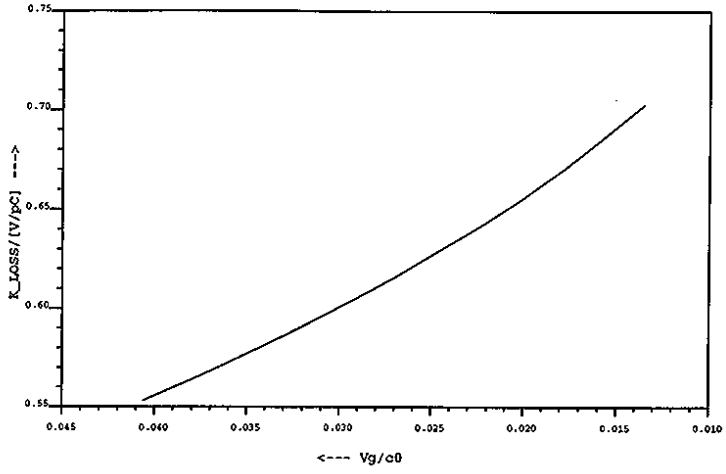

Figure 16: Single cell loss-paramter of the accelerating mode as a function of the group velocity.

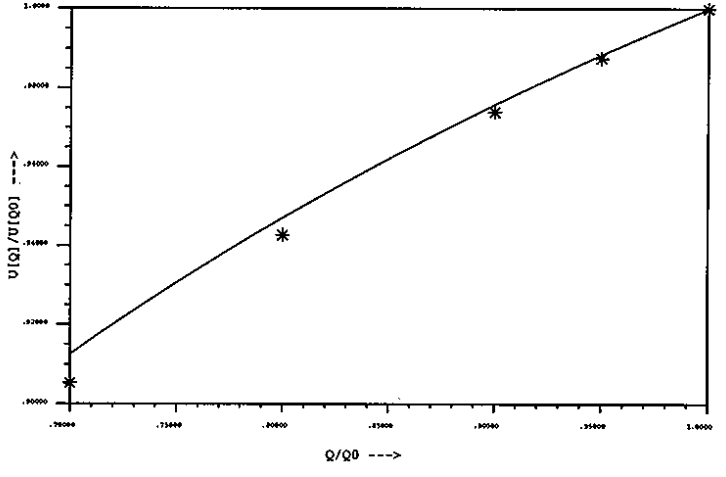

Figure 17: Reduced accelerating voltage caused by the Q reduction. Solid line: $< k_i >$ is taken as constant, *: effect of different tapering is taken into account. ($\tau_{\text{fill}} = 0.818\mu s := const.$)

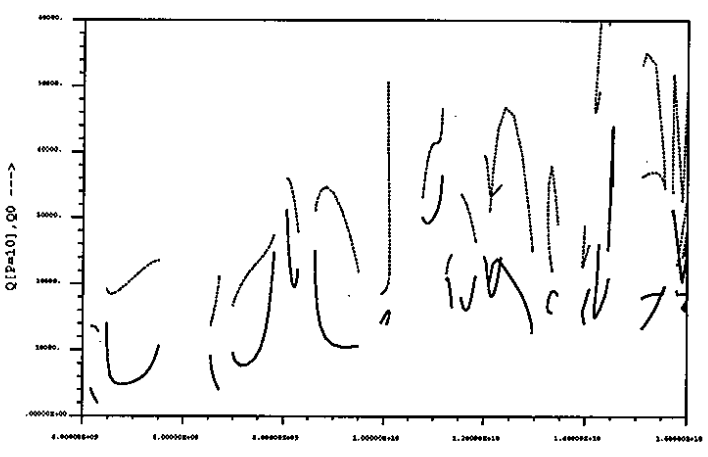

Figure 18: Single cell quality factors as function of frequency (phase advance) for higher dipole bands. MAFIA calculation for cell 25 ($v_g^{(m)}/c_0 = 3.7\%$) without coating (dashed line) and for $P = 10$ (solid line).

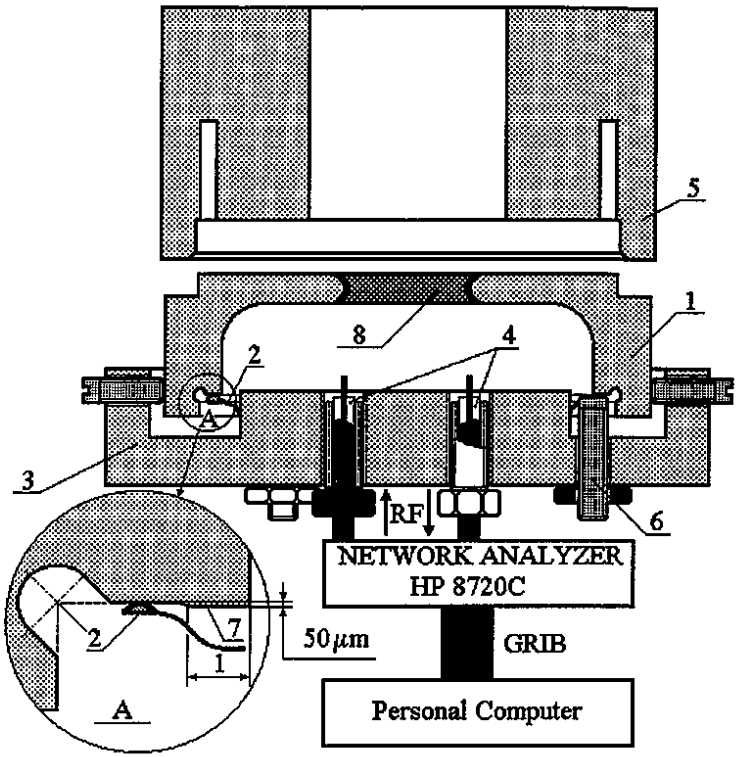

Figure 19: Single cell test resonator. (1 - cell under test, 2 - contact spring, 3 - bottom plate, 4 - antennas, 5 - body with cutoff pipe, 6 - support pivot (three pieces), 7 - contact edge, 8 - coated iris.)

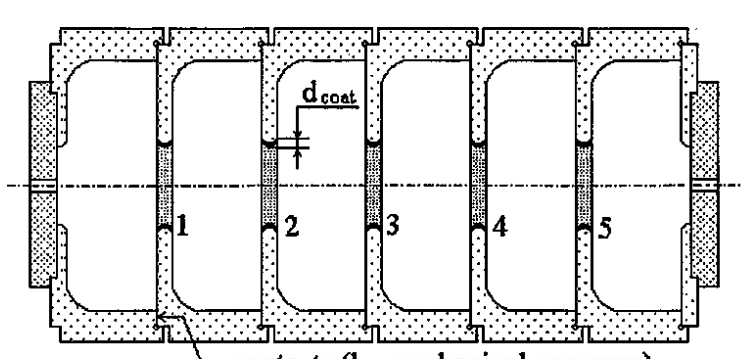

Figure 20: Six cell test resonator with five replacable cells.

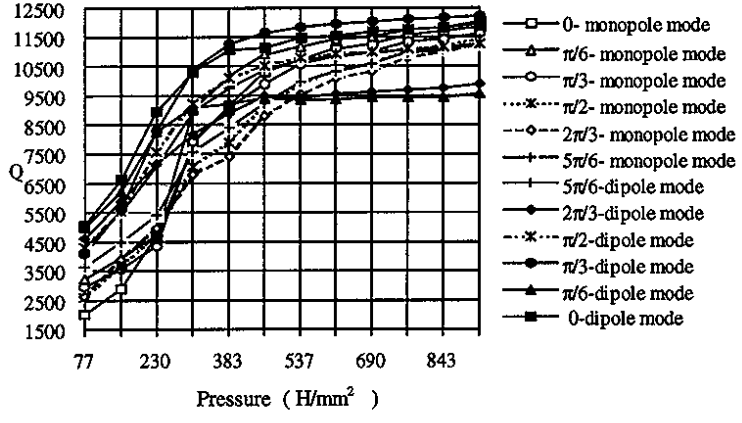

Figure 21: Quality factors of monopole and dipole modes in the six cell test resonator as a function of the contact pressure. (cell 25 with $v_g^{(m)}/c_0 = 2.2\%$, no iris coating)

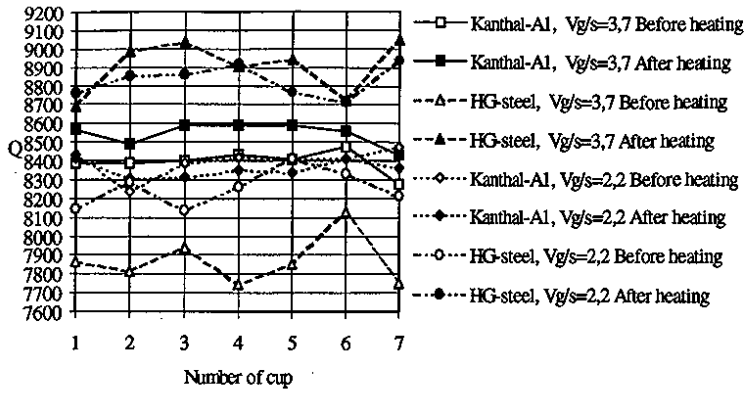

Figure 22: Monopole mode quality factors of iris coated cells measured in the one cell test resonator. (v_g/c_0=2,2% and 3,7%, d_{coat} = 1.5mm, coating materials: Kanthal and stainless steel)

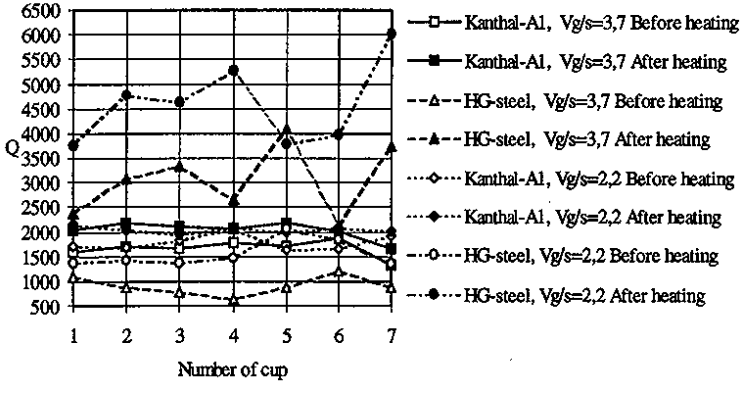

Figure 23: Dipole mode quality factors of iris coated cells measured in the one cell test resonator. (v_g/c_0=2,2% and 3,7%, d_{coat} = 1.5mm, coating materials: Kanthal and stainless steel)

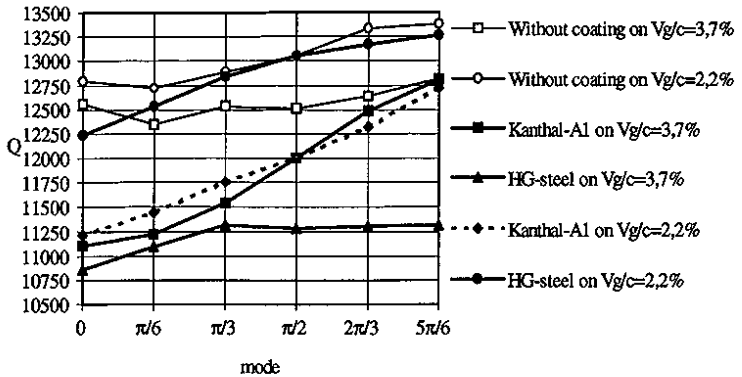

Figure 24: Monopole mode quality factors of five iris coated cells in the six cell test resonator. (v_g/c_0=2,2% and 3,7%, d_{coat} = 1.5mm, coating materials: Kanthal and stainless steel after heating)

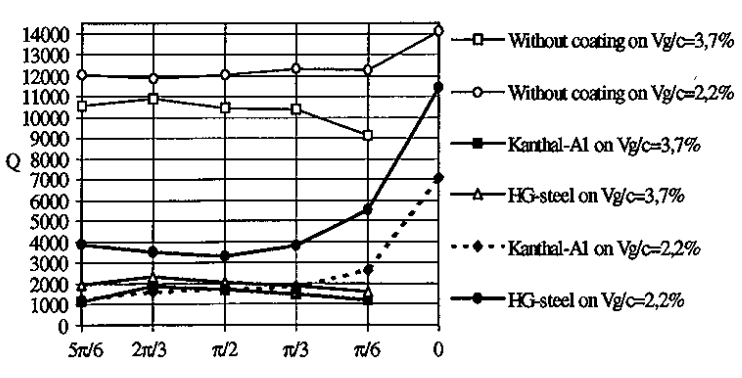

Figure 25: Dipole mode quality factors of five iris coated cells in the six cell test resonator. (v_g/c_0=2,2% and 3,7%, d_{coat} = 1.5mm, coating materials: Kanthal and stainless steel after heating)

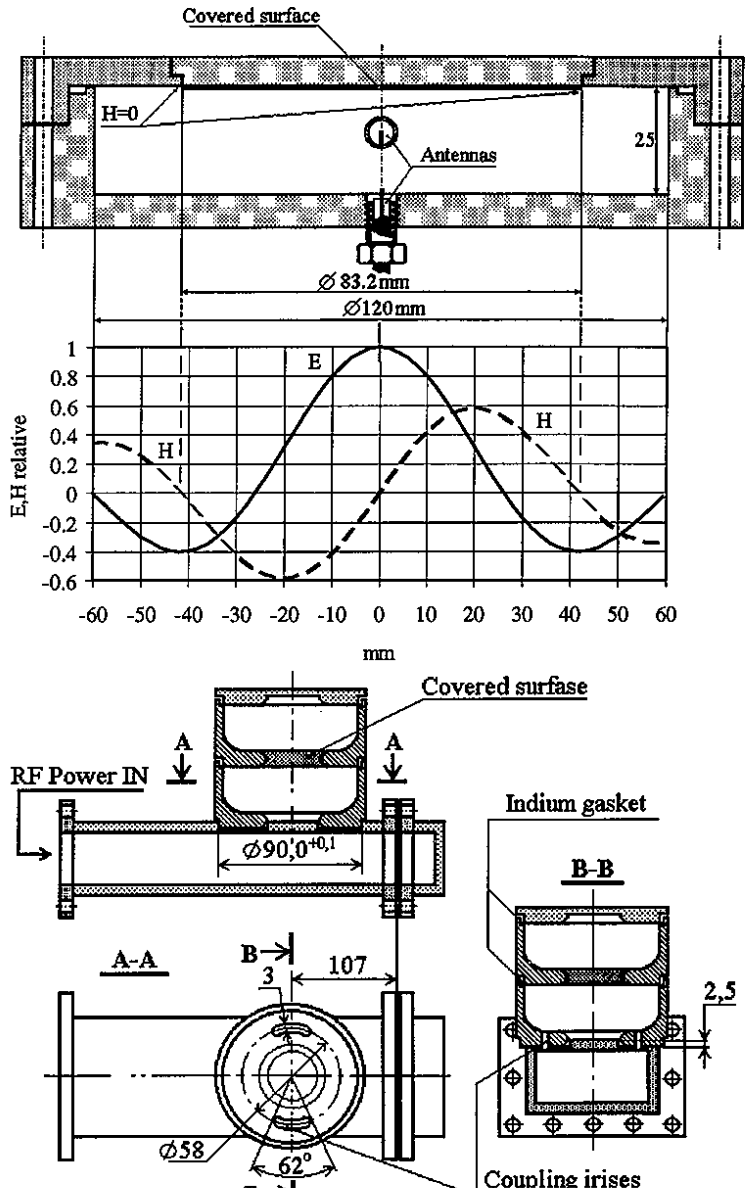

Figure 26: Test resonators: a) for a precise measurement of the surface absorption parameter P at low power conditions, b) for a high power test of SBLC cells.